NASA TECHNICAL NOTE

NASA TN D-8464

NASA TN D-8464

FLOW AND HEAT TRANSFER IN A CURVED CHANNEL

Paul F. Brinich and Robert W. Graham

Lewis Research Center

Cleveland, Ohio 44135

NATIONAL AERONAUTICS AND SPACE ADMINISTRATION • WASHINGTON, D. C. • MAY 1977

1. Report No.	2. Government Accession No.	3. Recipient's Catalog No.
NASA TN D-8464		

4. Title and Subtitle	5. Report Date
FLOW AND HEAT TRANSFER IN A CURVED CHANNEL	May 1977
	6. Performing Organization Code

7. Author(s)	8. Performing Organization Report No.
Paul F. Brinich and Robert W. Graham	E-9027
	10. Work Unit No.
	505-05

9. Performing Organization Name and Address	11. Contract or Grant No.
Lewis Research Center National Aeronautics and Space Administration Cleveland, Ohio 44135	
	13. Type of Report and Period Covered
	Technical Note

12. Sponsoring Agency Name and Address	14. Sponsoring Agency Code
National Aeronautics and Space Administration Washington, D.C. 20546	

15. Supplementary Notes

16. Abstract

A study of flow and heat transfer in a curved channel of aspect ratio 6 and inner- to outer-wall radius ratio 0.96 disclosed secondary currents and large longitudinal vortices. The heat-transfer rates of the outer and inner walls were independently controlled to maintain a constant wall temperature. Heating the inner wall increased the pressure drop along the channel length, whereas heating the outer wall had little effect. Outer-wall heat transfer was as much as 40 percent greater than the straight-channel correlation, and inner-wall heat transfer was slightly less than the straight-channel value. Overall heat transfer when both walls were heated was 22 percent greater than the straight-channel correlation.

17. Key Words (Suggested by Author(s))	18. Distribution Statement
Turbulent channel flow; Turbulent heat transfer; Secondary flow; Vortices; Pipe flow; Convective heat transfer; Contours	Unclassified - unlimited STAR Category 34

19. Security Classif. (of this report)	20. Security Classif. (of this page)	21. No. of Pages	22. Price*
Unclassified	Unclassified	39	A03

* For sale by the National Technical Information Service, Springfield, Virginia 22161

FLOW AND HEAT TRANSFER IN A CURVED CHANNEL

by Paul F. Brinich and Robert W. Graham

Lewis Research Center

SUMMARY

Flow visualization, pressure, velocity, temperature, and heat-transfer measurements were made in a curved channel having a rectangular cross section of aspect ratio 6, a ratio of inner- to outer-wall radius of 0.96, and an air inlet velocity range of 30.5 to 91.5 meters per second. This study showed that very little of the flow could be considered two dimensional and that large streamwise vortices formed on the inner wall. Heating the inner wall caused an increase in the channel pressure drop, whereas heating the outer wall had little effect. The principal changes in velocity profile occurred along the inner wall, where the large-vortex development took place. The friction coefficients along the outer-wall centerline were about 50 percent greater than the straight-channel correlation and were variably less along the inner-wall centerline, depending on the vortex structure. The outer-wall heat transfer was about 40 percent greater, and the inner-wall heat transfer was slightly less, than the straight-channel correlation. Overall heat transfer when both walls were heated was about 22 percent greater than the straight-channel correlation.

INTRODUCTION

Many applications of fluid mechanics and heat transfer involve curved surfaces or curved channels, for which the well-established principles of simple rectilinear flows do not apply. Curved flows are complicated by the presence of centrifugal and Coriolis forces and vortical motions, in addition to the usual inertial and viscous forces that characterize flows with nearly straight streamlines. Such complications in flows with curvature lead to extra rates of strain that are difficult to quantify and hence make accurate predictions of fluid flow and heat transfer difficult or impossible (ref. 1).

The present investigation into curved flows was stimulated several years ago in connection with rocket nozzle cooling and similar applications. Although the curved rocket nozzle cooling passages were known to have complicated three-dimensional flows

for which no analytical methods were expected to apply, it was thought that some attempt should be made to design an experiment in which the flow could be considered to be two dimensional so that some fundamental data could be obtained. Accordingly, a curved channel having an aspect ratio of 6 (cross section, 2.54 cm by 15.24 cm) and a radius of curvature of 66 centimeters and designed to have fully developed flow at its entrance was built. A long constant-area straight section preceded the curved channel to provide the desired entrance flow condition. The walls of the curved channel were capable of being heated to obtain heat-transfer information.

Since it was impossible to determine beforehand to what extent the curved channel would have two-dimensional flow, it was decided that this question should be resolved first, preferably by some visual technique that would reveal the gross flow patterns. This was then followed by flow and heat-transfer measurements and an attempt to correlate the various measurements with other experiments and theory.

Measurements were made and data taken in the U.S. customary system of units and converted to SI units for this report.

SYMBOLS

A	heat-transfer surface area
A'	cross-sectional area of channel
C_f	local friction coefficient
C_p	pressure coefficient
D	Preston-tube diameter
d	internal pipe diameter or channel width
d_h	hydraulic diameter of channel
M	Mach number
P	stagnation pressure
Pr	Prandtl number
p	static pressure
Q	total heat-transfer rate corrected for conduction losses
Re	Reynolds number
Re_D	Reynolds number based on Preston-tube diameter
Re_d	Reynolds number based on pipe diameter or channel width

Re_{dh}	Reynolds number based on channel hydraulic diameter
r	turning radius of channel
St	Stanton number
T	temperature
u	velocity in stream direction
x	linear distance in stream direction (flow distance)
y	distance perpendicular to channel walls
δ	boundary-layer thickness
γ	specific-heat ratio
θ	turning angle of channel (angular position, or station)
λ	friction factor
μ	absolute viscosity
ν	kinematic viscosity
ρ	air density
τ_w	shear at wall

Subscripts:

B	bulk
i	inner wall
max	maximum
min	minimum
o	outer wall
w	conditions at wall
0	inlet conditions
1	successive locations in flow direction
2	successive locations in flow direction
∞	conditions at outer edge of boundary layer

Superscript:

+	turbulent law-of-wall variables

APPARATUS AND INSTRUMENTATION

The pertinent dimensions and method of construction of the 2.54-centimeter by 15.24-centimeter curved channel are shown in figure 1. Also shown are the long, straight entrance section and the smoothly curved bellmouth, which were constructed of wood, and the short, straight downstream section, which was made of metal. Atmospheric air was admitted through a fiber-glass filter into the plenum and then through the channel and was discharged into a downstream vacuum source of about 3-N/cm^2 pressure. The flow was regulated by a gate valve ahead of the vacuum source to give inlet velocities of 30.5, 61.0, and 91.5 meters per second. Inlet velocities were determined from the total and static pressures near the inlet of the straight section. The channel radius of curvature was 66 centimeters and the total turning angle was 210°. Probe access ports were located at seven positions along the curved wall, separated by 30 degrees. Several access ports were also located in the upstream and downstream straight sections.

Construction details of the curved heat-transfer channel are shown in section A-A (fig. 1). Two copper walls 0.64 centimeter thick were curved to fit into grooves cut into the upper and lower Lucite walls and sealed with 0.32-centimeter-diameter silicone rubber strips. Spacing between the inner and outer copper walls was 2.54 centimeters ± 1 millimeter. The upper and lower Lucite walls in turn were sandwiched between the upper and lower steel plates, which were clamped together with long bolts to form a rigid structure. Figure 2 shows the channel with the insulation removed. Also shown are the probe actuator at the fifth angular position (station) and the many pressure and electrical leads required to transmit the data. The upper and lower steel plates, in addition, serve as a form about which hard board sheets could be bent to contain the loose Vermiculite insulation that was used to reduce extraneous heat losses when heat-transfer measurements were being made.

Each of the two copper walls was heated with seven individually controlled electric heater pads that were cemented to the exterior channel surfaces. Each heater pad occupied about 30 degrees of arc in length by 15 centimeters in width and was powered by a remotely controlled variable transformer. The heaters were constructed of silicone rubber with internal heating elements having a total thickness of about 0.75 millimeter and were designed for a maximum of 115 volts and 180° C. Suitable openings for probing stations, static pressure orifices, and thermocouples were provided in each heater. Thermistors were attached to each of the 14 heaters to monitor the heater temperature, which was not to exceed 180° C. Heater power was determined from the voltage drop across the heater terminals and the current in the power leads and was used to determine the heat transfer into each segment of the channel walls. Heater power was measured with an estimated error of about ±2 percent and was assumed to be uniformly distributed over the area covered by the heater. These measurements were then corrected

for conduction heat losses through 5 centimeters of wall insulation. The heat losses ranged from about 1/2 percent at 91.5 meters per second to 1 percent at 30.5 meters per second.

Wall static pressures were measured at 55 locations along the centerlines of the channel side walls, of which 42 were on the curved walls. These pressures were measured with oil-filled manometers (specific gravity, 0.82) and were read to an accuracy of ±0.15 centimeter. Wall temperatures were measured at 28 locations long the centerlines of the curved copper walls with Chromel-Alumel thermocouples and were read with an accuracy of ±1 degree C.

Total pressure, velocity, and temperature profiles were measured at each of the seven probing stations with the probes shown in figure 3. The probes were double headed to permit measurements close to both the inner and outer walls without the necessity of changing probes and were used with the channel operated in the adiabatic condition as well as heated. Pressures were sensed by a 0.7-N/cm^2 differential transducer that was referenced to the local outer-wall static pressure and were recorded on a two-pen x-y recorder. To insure good accuracy, the transducers were calibrated against an oil manometer in the appropriate pressure ranges for the three velocities investigated. The probable pressure errors as a result were less than 1 percent.

Total temperature recovery for the temperature probes shown in figure 3 was assumed to be unity since the stream velocities were in the low-subsonic range. Based on the output of the Chromel-Alumel thermocouple and the reading accuracy of the recorder traces, temperature errors were of the order of ±0.5 degree C. Conduction from the heated walls and convection from the hot stream into the probe support, however, may have affected the temperatures sensed by the thermocouple junction at the probe tip. These effects were not evaluated.

Inner- and outer-probe positioning errors relative to their respective walls were within ±0.4 millimeter, and wall contact of the probes was established with a sensitive ohmmeter. Preston-tube pressure measurements were made with the total pressure survey probes in contact with the inner and outer walls.

To facilitate changing of the probes, the Vermiculite insulation was not used when the movable probes were installed. Rather, the same wall temperature was set as was obtained in the heat-transfer tests when the insulation was present.

In making the visual studies of the flow, the copper walls shown in figure 1 were replaced with transparent plastic walls of the same thickness. Only static pressure instrumentation was installed on the plastic walls and consisted of seven vertical rows of five orifices at each of the seven probing locations on each wall.

RESULTS

Flow Visualization

Before the fluid flow and heat transfer in the curved channel were measured quantitatively, two attempts at visualizing the flow were made. The copper walls shown in figure 1 were replaced with transparent plastic walls, and colored water was introduced through the five static pressure orifices located on each side wall near the entrance to the curved section. The colored water was introduced slowly enough to form long narrow streamers that remained attached to the walls and that could be followed by eye to determine the flow direction down the channel. In brief, the streamers indicated diverging flow on the outer (concave) wall and converging flow along the inner (convex) wall. Attempts were made to photograph the streamers, but success was marginal.

Accordingly, a second attempt was made to record the flow patterns on the wall. Sheets of smooth white plastic with pressure-sensitive backing (contact paper) were attached to the two side walls and to the top and bottom walls. A mixture of lampblack in linseed oil was used to show the flow direction on the four walls. The mixture was applied to the white plastic in straight lines normal to the general flow direction with a draftsman's ruling pen at seven stations down the curved channel (the stations being 30 degrees apart). The channel was then assembled and the flow was started at the 61.0-meter-per-second speed and allowed to run for about 5 minutes. During this time, black streaks developed from each of the normal lines, indicating the local flow patterns against a white background. The patterns thus established were allowed to dry about 24 hours, the channel was disassembled, and the plastic sheets were removed from the walls. The flow patterns at selected stations were photographed and are displayed in figure 4.

The flow patterns on the outer wall showed a fairly uniform distribution of lines with negligible variation between stations. Hence, traces for only two stations are shown. Flow divergence on the outer wall is hardly noticeable and contrasts with the flow patterns along the inner wall, which converge noticeably and are far from uniform. The flow angularity along the top and bottom walls, also shown in figure 4, is even more dramatic evidence of the strong crossflows that existed in the channel.

The nearly uniform distribution of lines on the outer wall is indicative of a uniform distribution of shear at the wall. Differences in line length are probably due to small longitudinal vortices caused by the concave turning. The streak patterns on the inner wall are less uniform and, because of their shorter length, they suggest reduced shear. Also to be noted is the absence of streaks in certain areas, which can be interpreted as the formation of fairly large, slow-moving longitudinal vortices on the inner wall. Thus, at the 45° station, there are two regions of low shear, suggesting the presence of two vortex pairs. At the 75° and 135° stations the center region only is free of streaks,

suggesting the existence of one large vortex pair between these stations. Finally, at the 165° station the shear has become more uniform again. Some of these flow characteristics are shown in figure 5 and will be recalled again when the flow and heat-transfer measurements are discussed.

Pressure Distribution Along Channel

The static pressure distributions were measured along the centerlines of the inner and outer walls, beginning at the inlet of the straight section and continuing to the discharge of the curved channel. This was done at inlet velocities of 30.5, 61.0, and 91.5 meters per second at adiabatic and heated wall conditions and an air inlet temperature of 24° C. The adiabatic wall condition was also 24° C, and the heated curved walls were maintained at a constant temperature of 93° to 110° C along the channel length, the higher temperatures being maintained at the lower velocities. In addition to both channel walls being heated simultaneously, they were also heated individually to study their independent contributions.

Wall static pressure distributions are expressed in coefficient form

$$C_p = \frac{p - p_0}{P - p_0}$$

where p is the static pressure along the wall, p_0 the static pressure in the straight channel near the inlet, and P the stagnation pressure at the inlet. Distributions of C_p for the adiabatic case are plotted at 30.5, 61.0, and 91.5-meter-per-second air inlet velocities in figure 6. A comparison of the distributions shows negligible differences between the 61.0 and 91.5-meter-per-second velocities and a slightly steeper pressure gradient for the 30.5-meter-per-second velocity. The straight-channel distributions indicate equal pressures on both channel walls except near the end of the straight section, where the effect of the curved-channel begins. At the start of the curved section an abrupt increase in pressure occurred for both the inner and outer curved walls. This pressure increase resulted from the force required to change the stream direction from rectilinear to curved flow. It is typical of similar experiments, such as those of references 2 and 3, except that in those instances the inner-wall pressures did not increase. The reason for this is believed to be the lower ratio of inner- to outer-wall curvature radius ($r_i/r_o = 0.8$ and 0.9) as compared with the present study ($r_i/r_o = 0.96$).

In addition to the sudden pressure rise at the start of the curved section, there is another sudden pressure rise at a linear flow distance x of about 330 centimeters. This second rise appears to be related to a change in the longitudinal vortex development

at the 75° ($x \approx 325$ cm) position discussed in the section Flow Visualization. It is also mentioned later when the boundary-layer profiles are presented.

Beginning at the curved section, there is a nearly constant pressure difference between the inner and outer channel walls of

$$C_{p,o} - C_{p,i} \approx 0.08 \text{ to } 0.10$$

regardless of velocity. This change in the pressure coefficient compares favorably with the expression for pressure differences in a curved flow field caused by centrifugal forces

$$\frac{dp}{dr} = \frac{\rho u^2}{r} \tag{1}$$

Integrating this expression and assuming the dynamic pressure to have a constant value $\rho u_0^2/2$ yields a pressure difference between the outer and inner walls of

$$\Delta p = \rho u_0^2 \ln\left(\frac{r_o}{r_i}\right) = 0.077\left(\frac{\rho u_0^2}{2}\right) \tag{2}$$

The pressure difference can be written in terms of the pressure coefficient as

$$\Delta p = (C_{p,o} - C_{p,i})\left(\frac{\rho u_0^2}{2}\right) \tag{2a}$$

and $C_{p,o} - C_{p,i} = 0.077$, which compares favorably with the previously measured values of 0.08 to 0.10.

The effect of heating the curved channel walls on the pressure coefficient can be seen by comparing the 61.0-meter-per-second results for the adiabatic condition in figure 6(b) with the heated-wall results shown in figures 7 to 9. In the straight unheated section, the pressure distributions were identical, whether or not the curved walls were heated. In the curved section the pressure drop on both walls increased when the inner and outer walls were heated simultaneously (compare figs. 6(b) and 7). Likewise, when only the inner wall was heated (fig. 8), there was a similar increase in pressure drop for both walls. However, when only the outer wall was heated (fig. 9), there was a negligible change in pressure drop in spite of the much larger heat-transfer rate necessary

to maintain a given temperature on the outer wall. Also, it was observed that the temperature rise at the downstream end of the inner wall when only the outer wall was heated was appreciably greater than the temperature rise of the outer wall when only the inner wall was heated to the same temperature (14° C vs. 5° to 6° C).

These results are indicative of the greater stability of the flow on the inner wall as compared with the outer. Thus, the air that is heated by the inner wall forms a coherent stable mass that shows little tendency to mix with the main flow. The flow that is heated by the outer wall, on the other hand, rapidly mixes with and gives up its heat to the mainstream. By remaining in contact with the inner wall when it is heated, the inner-wall flow forms a constriction in the channel that increases the pressure drop. Hence, the smallest pressure drop will occur if only the outer wall is heated and, for the conditions of this experiment, was seen to approximate the adiabatic pressure drop. Although these results pertain to the 61.0-meter-per-second data, similar results were also found at the 30.5 and 91.5-meter-per-second velocities.

Friction Factors

The friction factor for fully developed flow in a circular pipe is defined in reference 4 by

$$\lambda = \left(\frac{p_1 - p_2}{x_1 - x_2}\right)\frac{d}{\left(\frac{\rho u_0^2}{2}\right)} \tag{3}$$

where d is the internal pipe diameter. This expression has been shown to be valid (ref. 4) for a straight pipe or channel of noncircular cross section if the diameter is replaced by the hydraulic diameter defined by

$$d_h = \frac{4 \times \text{Section area}}{\text{Wetted perimeter}}$$

For the present experiment, the hydraulic diameter is 4.35 centimeters.

Friction factors were obtained by measuring the slopes of the straight lines that are faired through the results in figures 6 to 9 and substituting them into the relation

$$\lambda = \left(\frac{C_{p,1} - C_{p,2}}{x_1 - x_2}\right)d_h \tag{3a}$$

which follows from the preceding equations and the definition of C_p. In an effort to select data in a region where the flow was well developed, only points for the downstream parts of the straight and curved sections of the channel were used in the fairings. The results for the straight and curved sections are shown in figure 10 for the four curved-wall conditions: adiabatic, outer wall heated, inner wall heated, and both walls heated. These results are compared to the empirical expression for a straight circular pipe given in reference 4,

$$\lambda = 0.316 \left(\frac{u_0 d}{\nu} \right)^{-0.25} \tag{4}$$

and represented by the straight lines in figures 10(a) and (b).

In general, the experimental points are higher than given by this relation, especially for the curved section, and tend to remain constant with changes in Reynolds number rather than to follow the slope of the empirical curve. This is somewhat surprising for the straight section and suggests that the characteristics of the curved section may be propagating upstream. The high values of λ and their constancy with Reynolds number for the curved section perhaps have their explanation in the results found for roughened straight pipes (ref. 4). In these results, the friction factor rose above the smooth-pipe turbulent level and approached a constant value as the Reynolds number was increased. This implies that, in a curved channel, there is an increase in turbulence and/or secondary flows that causes an increase in mixing, similar in effect to the increased mixing caused by roughness in a straight pipe.

The effect of wall heating on the pressure coefficient discussed earlier can also be seen in the friction factor for the curved channel (fig. 10(b)). Heating only the inner wall caused a significant increase in λ, whereas heating only the outer wall resulted in the same friction factor as for the adiabatic case. Heating both walls resulted in a slightly higher friction factor than heating only the inner wall. The straight section was unheated but reflects some of the characteristics of the heated curved section, as indicated in figure 10(a).

Velocity and Temperature Profiles

Velocity and temperature profiles were measured at each of the seven stations at inlet velocities of 30.5, 61.0, and 91.5 meters per second. Velocity profiles were measured for the adiabatic and heated wall conditions, but temperature profiles were measured at the heated wall condition only. However, no velocity or temperature profiles will be presented for heating of only the inner or outer wall. Again, the results

found at 61.0 meters per second are presented in greater detail since these are typical, although some comparisons of the different velocities are made.

Velocity profiles for the adiabatic and heated wall conditions are shown in figures 11 and 12 at an inlet velocity of 61.0 meters per second. They are shown shifted downward 0.1 unit to prevent overlapping of the plots. Peak values occur at a velocity ratio of unity for each profile. The velocities were calculated by assuming the flow to be compressible and were referenced to the maximum velocity at each measuring station. The maximum velocities u_{max} at the various stations in figures 11 and 12 were approximately constant and ran about 10.5 meters per second greater than the inlet velocity for the adiabatic case and 11.5 meters per second greater for the heat-transfer case. When the walls were heated, the measured temperature distributions at each station were used to find the velocity ratio, which is given by

$$\frac{u}{u_{max}} = \frac{M}{M_{max}} \sqrt{\frac{T}{T_{min}}} \tag{5}$$

Because of the low velocities, the temperature T was assumed to be equal to the probe reading without any recovery correction. The Mach number was obtained from the ratio of static to total pressure, where the static pressure was calculated from a linear interpolation of the inner and outer wall static pressures

$$M = \sqrt{\frac{2}{\gamma - 1}\left\{\left[\frac{P(y)}{p(y)}\right]^{(\gamma-1)/\gamma} - 1\right\}} \tag{6}$$

That the actual static pressure distribution was approximately linear was verified by integrating equation (1) at two typical curved-wall stations. The velocity profiles have a continuously changing shape beginning with a nearly symmetric profile at the exit of the straight section, followed by two profiles having peaks near the inner wall, and then changing to profiles having peaks nearer the outer wall. The difference between the adiabatic and heat-transfer profiles is primarily on the inner (convex wall) portion of the profile, which indicated higher velocity ratios for the heat-transfer condition.

This progression of profile development can be readily correlated with the flow traces in figure 4 and the pressure distribution in figure 6. At angular positions (stations) θ of 15° and 45° (fig. 4), the longer flow traces near the centerline on the inner wall show a relatively large shear, whereas at 75° and 135° the shear is appreciably diminished. This is borne out by figures 11 and 12, where the profiles at 75° change

quite abruptly. In figure 6, there are three discontinuities in the pressure distribution. The first occurs at the entrance to the curved channel ($x \approx 254$ cm; $\theta = 0^{\circ}$), the second at $x \approx 318$ centimeters ($\theta = 75^{\circ}$), and the third at $x \approx 380$ centimeters ($\theta = 135^{\circ}$). At each of these points the profiles exhibit changes in secondary flow patterns and in the number of large vortices that form in the curved channel. Some of these flow features can be readily identified in the vortex patterns sketched in figure 5.

Temperature profiles measured when the inner and outer channel walls were heated simultaneously are presented in figure 13 in terms of the ratio $(T_w - T)/(T_w - T_{min})$. As was the case for the velocity profiles, each successive profile is shifted downward 0.1 unit to avoid confusion in plotting; that is, the peaks all occur at a ratio of unity. Average wall temperatures were 106° C, with individual variations of ±2 degrees C. Except for the first profile at $\theta = 15^{\circ}$, which is near the start of the thermal layer, and the inner-wall portion of the last four profiles, the temperature profiles are quite similar to the velocity profiles. Apparently, the large-scale vortex development toward the downstream end of the inner wall tends to modify the implied Reynolds analogy between momentum and heat transfer in this region.

Earlier it was stated that the velocity and temperature profiles obtained at 30.5 and 91.5 meters per second were nearly the same as those shown in this report at 61.0 meters per second. The profiles at the middle station ($\theta = 105^{\circ}$) for the adiabatic and heated walls are compared in figures 14(a) and (b). In general, the 30.5-meter-per-second velocity profiles were slightly lower near the walls and the 91.5-meter-per-second profiles were slightly higher near the walls than the 61.0-meter-per-second profiles. These differences are minor and are probably Reynolds number effects.

Skin Friction (Preston-Tube Results)

Although the friction factor results presented earlier gave an indication of the average flow resistance in the channel, they did not account for the variations along the channel nor the differences in friction between the inner and outer walls. To get an estimate of the local friction coefficient in the curved channel, the simplified Preston-tube technique of reference 5 was used. To find the friction coefficient C_f by the method of reference 5, it was only necessary to know (1) the velocity ratio u/u_{max} when the Preston tube was in contact with the wall and (2) the probe Reynolds number $Re_D = u_{max}D/\nu$. The location of the point defined by these coordinates on a family of curves plotted in reference 5 defines the friction coefficient directly. The boundary-layer pitot pressure probe served as the Preston tube when it was in contact with the wall.

Preston-tube skin friction results are presented for the adiabatic and heated channels in figures 15 and 16 in terms of friction coefficient C_f and Reynolds number Re_d, which are defined as

$$C_f = \frac{\tau_w}{\left(\frac{\rho u_{max}^2}{2}\right)}$$

$$Re_d = \frac{\rho u_{max} d}{\mu}$$

The use of u_{max} rather than u_0 in the definition of Reynolds number was to keep the definition of friction coefficient and Reynolds number consistent with each other. If u_0 were used to calculate Reynolds number in figures 15 and 16 instead of u_{max}, the experimental points would be moved to the left slightly, resulting in a negligible change in the correlation. The velocities u_{max} and u_∞ are considered to be equal.

Figures 15(a) and 16(a) show that for the outer wall the friction coefficients for the first two stations were at a level consistent with the empirical correlation for a straight pipe adapted from reference 4

$$C_f = 2\left(\frac{\tau_w}{\rho_\infty u_\infty^2}\right) = \frac{2 \times 0.0225}{\left(\frac{u_\infty \delta}{\nu}\right)^{0.25}} = \frac{0.045}{\left(\frac{1}{2}\right)^{0.25}\left(\frac{u_\infty d}{\nu}\right)^{0.25}} = \frac{0.054}{\left(\frac{u_\infty d}{\nu}\right)^{0.25}} \tag{7}$$

This was followed by rather high values at the next six stations, which were independent of distance downstream but showed a definite variation with Re_d (channel velocity level). Such behavior along the outer wall is characteristic of fully developed channel flow even though the velocity profiles along the inner wall were showing large changes in their downstream development. The increase in outer-wall C_f over the empirical equation was about 50 percent. Differences between the adiabatic and heat-transfer channel flows were minimal.

Friction coefficient variations along the inner wall shown in figures 15(b) and 16(b) contrast with those for the outer wall. In general, there was a rapid drop in C_f in going from the straight-channel value at an x of 213 centimeters to θ of 15°, 45°, and 75°. These changes in C_f are related to the profound changes of the inner-wall velocity profiles noted earlier, which are in turn related to changes in vortex patterns. Beyond $\theta = 75^\circ$ the friction coefficient gradually rose to near its initial value with increasing distance downstream, suggesting a tendency toward an equilibrium state, perhaps 15 percent below the empirical straight-pipe value. Again, differences between adiabatic and heated-wall flows were slight.

Universal Velocity Profiles (Logarithmic Forms)

The velocity profiles shown in figure 10 for the adiabatic flow at 61 meters per second were converted to the universal turbulent law-of-the-wall form (ref. 4) by using the friction coefficients plotted in figure 15 and are shown in figure 17. The law of the wall is expressed by

$$u^+ = A \log y^+ + B \tag{8}$$

where

$$u^+ = \frac{u}{u_\infty}\sqrt{\frac{2}{C_f}} = \frac{u}{u_{max}}\sqrt{\frac{2}{C_f}}$$

and

$$y^+ = \frac{u_\infty y}{\nu}\sqrt{\frac{C_f}{2}} = \frac{u_{max} y}{\nu}\sqrt{\frac{C_f}{2}}$$

and where A and B are constants that were taken as 5.75 and 5.5, respectively, as suggested in reference 4 and were used to establish the straight lines in figure 17.

Figure 17 shows that while the experimental results for the straight channel tend to agree with the universal profile of reference 4 over the full extent of the profile, the agreement for the curved-channel profiles extends out only to about $\log y^+ \sim 2.4$. The outer-wall profiles in figure 17(a) then drop below the universal profile and the inner-wall profiles of figure 17(b) rise above it. This general behavior of the turbulent curved-channel flow was also observed in reference 2 at velocity levels that were one-third of the present and a channel radius ratio r_i/r_o of 0.8, as compared with 0.96 for the present study.

Some features of figure 17 should be noted. The first curved-channel profile ($\theta = 15^o$) for the outer wall rises above all the following profiles in the outer region, suggesting that the flow is in a state of transition between straight-channel flow and curved-channel flow. Beginning at $\theta = 45^o$, all the outer-wall profiles are similar. The inner-wall profiles, on the other hand, do not become similar until $\theta = 135^o$, which is downstream of the last discontinuity in the static pressure distributions shown in figure 6. The profile at $\theta = 75^o$ reaches a peak at $u^+ = 33$. This station corresponds to

the position at which the large double vortex along the inner wall was believed to originate.

A general observation drawn from figure 17 is that the profiles appear similar to those observed in boundary layers developing in accelerating and decelerating flows, respectively (e.g., flow in a convergent-divergent channel, ref. 6). The present experiment, however, involves essentially a nonaccelerating flow with equal pressure gradients on the inner and outer walls. Therefore, the characteristic shape of the profiles must be attributed to curvature and secondary flow effects.

Heat Transfer

Heat-transfer measurements were made in the curved channel at three inlet velocities and three heat-transfer arrangements: (1) outer wall heated, (2) inner wall heated, and (3) outer and inner walls heated simultaneously. Temperature variations along the walls were usually maintained at ±3 degrees C for each test condition and varied from 110° C at the lowest velocity to 102° C at the highest. Room-temperature air entered the inlet at 21° to 25° C.

The heat-transfer results are presented in terms of the Stanton number St, which is defined as

$$St = \frac{Q}{\rho_0 u_0 C_p A(T_w - T_B)} \tag{9}$$

where Q is the electric power into a wall segment corrected for the conduction heat loss through the outside insulating layer, A is the area of the wall segment, T_w is the wall temperature, and T_B is the stream bulk temperature. The bulk temperature was found from a knowledge of the inlet temperature T_0, the heat input to the stream, and the mass flow through the channel. Thus, the bulk temperature for the center of the n^{th} heater is given by

$$T_{B,n} = T_0 + \frac{1}{\rho_0 u_0 C_p A'}(Q_1 + Q_2 + \ldots + Q_n/2) \tag{10}$$

where A' is the cross-sectional area of the channel and $Q_1, Q_2, \ldots, Q_n/2$ are the corrected electric power into each heater. When both walls were heated simultaneously, the power input from both walls was used to find $T_{B,n}$.

Figures 18 and 19 present the heat-transfer results in terms of Stanton and Reynolds numbers for the outer and inner curved walls, respectively. These results are

compared with the empirical relation given in reference 7 for heat transfer in a straight tube but with the Reynolds number based on the hydraulic diameter d_h rather than on a physical tube diameter d:

$$St = \frac{0.0396}{Re_{dh}^{0.25}\left(1 - \frac{0.44}{Re_{dh}^{0.125}}\right)} \tag{11}$$

The present results show an average Stanton number increase of about 40 percent over the straight-tube correlation for the outer wall when both walls were heated (fig. 18(b)) and a lesser increase of 26 percent when only the outer wall was heated (fig. 18(a)). The inner-wall comparisons are shown in figure 19 and indicate only a small reduction in Stanton number as compared with the straight tube. When the combined heat transfer from the inner and outer walls was used to calculate the Stanton number, the results shown in figure 20 were obtained. In this case, the heat-transfer increase over the reference 7 line was about 22 percent.

When the ratio of the outer- to the inner-wall heat transfer was calculated, the results shown in figure 21 for the various stations along the curved channel were obtained. These show that the largest ratios were obtained at the highest velocities (i.e., the highest Reynolds numbers) when both walls were heated simultaneously and at angular stations θ of 75° or more. The variation with Reynolds number is believed to be caused by conductive heat leakage through the channel insulation that is constant regardless of Reynolds number, whereas the convective heat transfer is proportional to the mass flow.

Heat-transfer ratios are predicted in reference 8 for a curved channel having a curvature ratio r_i/r_o of 0.958 (as compared with the present ratio of 0.962) at various Prandtl and Reynolds numbers. The ratio predicted for $Re_d = 10^5$ (2×10^5 in the nomenclature of ref. 8) and unity Prandtl number is 1.55, which is to be compared with the present value of about 1.5 when both walls are heated.

SUMMARY OF RESULTS

The present study of the flow and heat transfer in a two-dimensional curved channel having an aspect ratio of 6 and a radius ratio of 0.96, operating at air inlet velocities of 30.5, 61.0, and 91.5 meters per second, and having adiabatic and heated walls gave the following general results:

1. The flow cannot be considered to be two dimensional since rather strong cross-flows from the outer to the inner walls were observed on the upper and lower channel

boundaries over the entire length of the curved channel. A large, slowly rotating vortex pair appeared to form along the centerline of the inner wall downstream of the entrance region of the curved wall.

2. Wall pressure coefficients were substantially the same at all three velocities. At the junction of the straight and curved channels, there was a sudden rise in static pressure, which indicated a discontinuity in acceleration, followed by a decline at about the same slope as for the straight channel, with the outer wall at a slightly higher pressure than the inner. Heating the outer wall had little or no effect on the slope of the pressure drop, whereas heating the inner wall increased the pressure drop. The explanation for this behavior can be found in the reduced mixing (increased stability) of the flow along the inner wall, which causes an increased constriction of the flow downstream in the channel and a consequent pressure rise.

3. Friction factors were approximately constant with Reynolds number for both the straight- and curved-channel flows. Friction factors reflected the static pressure variations when the walls were heated; that is, the friction factor increased when the inner wall was heated and remained unchanged when only the outer wall was heated.

4. Dimensionless velocity profiles obtained at the three velocity levels for a given station were virtually congruent except for minor differences very close to the walls. When both channel walls were heated, appreciable velocity ratio increases occurred for the inner-wall profile as compared with slight increases for the outer-wall profiles. A comparison of the velocity and temperature profiles indicated approximate similarity at the 45° and 75° stations. Before the 45° station the thermal boundary layer was in a state of early development, whereas the velocity profile was well developed, and similarity would not be expected. Beyond the 75° station, the inner-wall profile was dominated by the accumulation of low-velocity air in the large-vortex pair along the inner-wall centerline, and again similarity would not be expected. For the outer wall, there was approximate similarity between the thermal and velocity profiles throughout the channel.

5. Preston-tube friction measurements on the outer curved wall showed increases of about 50 percent over the straight-channel values and very little effect of heat transfer. Friction measurements on the inner curved wall generally fell below the values for the straight channel and could be correlated with the vortex development along the inner wall. When plotted in universal (law of the wall) coordinates, the outer-wall profiles formed a family of profiles below the law-of-the wall line, and the inner-wall profiles a family above the line. This behavior is typical of results found in other curved-channel studies, and the trends have been predicted from theoretical considerations.

6. Heat-transfer measurements on both the inner and outer walls in general showed the characteristic decline of Stanton number with increasing Reynolds number observed in straight channels. The outer-wall heat transfer showed an average increase of 26 to

40 percent over the straight-channel correlation, and the inner wall a slight decrease. When the heat transfers from the inner and outer walls were combined, there was only a 22 percent increase in total heat transfer over the straight-channel correlation. The ratio of the outer- to the inner-wall heat transfer for a Reynolds number of 10^5 at a downstream station θ of 75° is roughly 1.50, which agrees well with a predicted value of 1.55.

Lewis Research Center,
National Aeronautics and Space Administration,
Cleveland, Ohio, January 12, 1977,
505-03.

REFERENCES

1. Bradshaw, P.: Effects of Streamline Curvature on Turbulent Flow - N74-12042, p. 274. Applied to Boundary Layer Conditions on Wing Sections and Turbomachine Blades. AGARDOGRAPH-169, Imperial Coll. Sci. Tech. (London), 1973.

2. Wattendorf, Frank L.: A Study of the Effect of Curvature on Fully Developed Turbulent Flow. Proc. R. Soc. London, Ser. A, vol. 148, 1934, pp. 565-598.

3. Eskinazi, Salamon; and Yeh, Hsuan: An Investigation of Fully Developed Turbulent Flows in a Curved Channel. J. Aeronaut. Sci., vol. 23, 1956, pp. 23-34.

4. Schlichting, Hermann: Boundary Layer Theory. McGraw-Hill Book Co., Inc., 1955, pp. 401, 406, 407, and 414.

5. Head, M. R.; and Ram, V. Vasanta: Simplified Presentation of Preston Tube Calibration. Aeronaut., vol. 22, no. 8, Aug. 1971, pp. 295-300.

6. Brinich, Paul F.; and Neumann, Harvey E.: Some Characteristics of Turbulent Boundary Layers in Rapidly Accelerated Flows. NASA TN D-6587, 1971.

7. Eckert, E. R. G.: Introduction to the Transfer of Heat and Mass. McGraw-Hill Book Co., Inc., 1950, p. 112.

8. Kreith, Frank: The Influence of Curvature on Heat Transfer to Incompressible Fluids. Trans. ASME, vol. 77, no. 11, Nov. 1955, pp. 1247-1256.

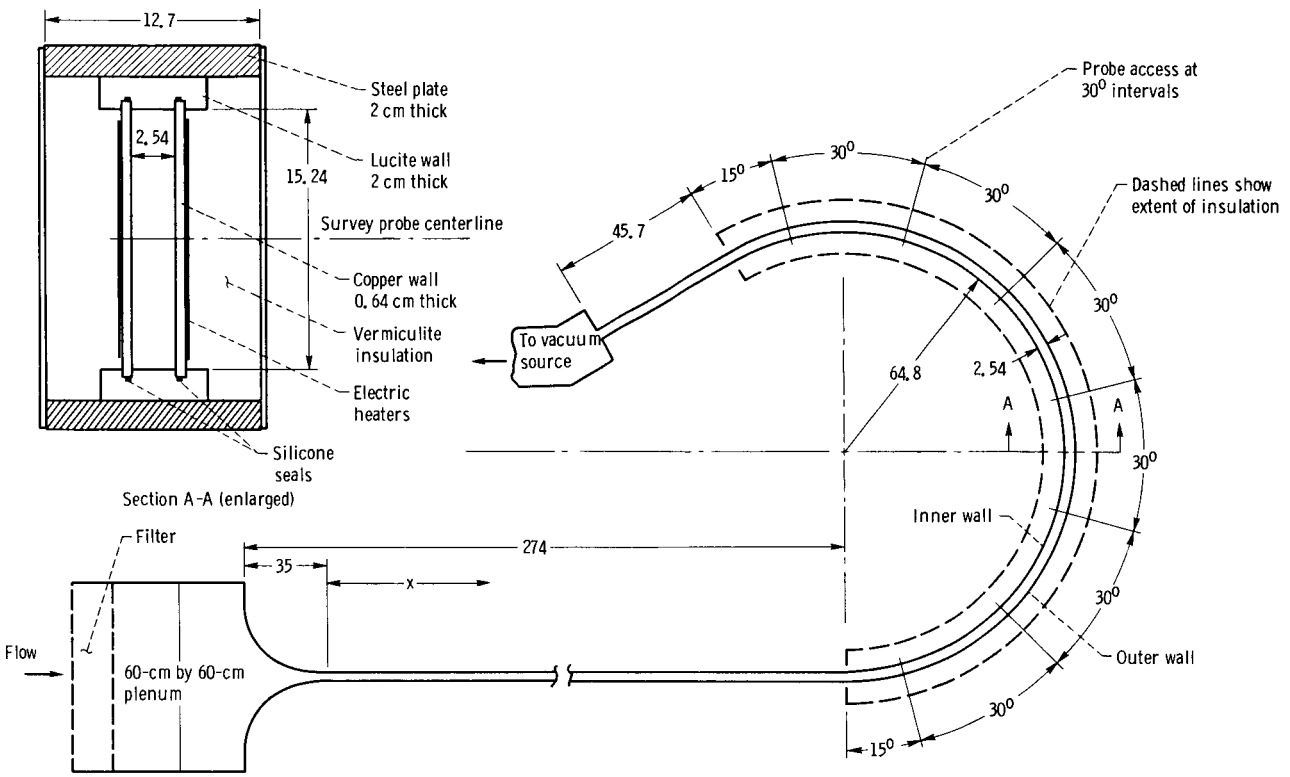

Figure 1. - Layout of curved heat-transfer channel. (Dimensions are in centimeters and degrees.)

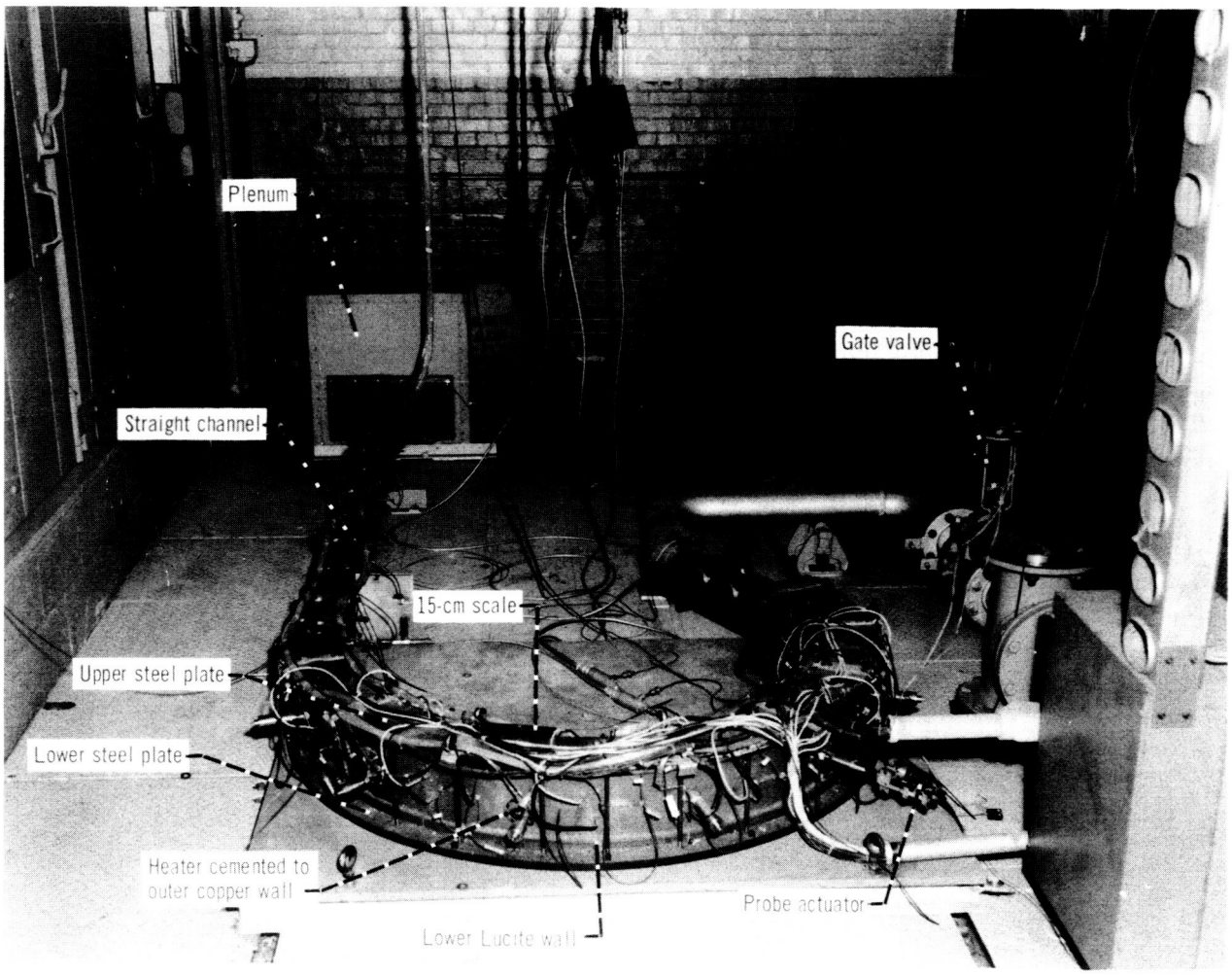

Figure 2. - Curved-channel apparatus with insulation removed and probe at 165° station.

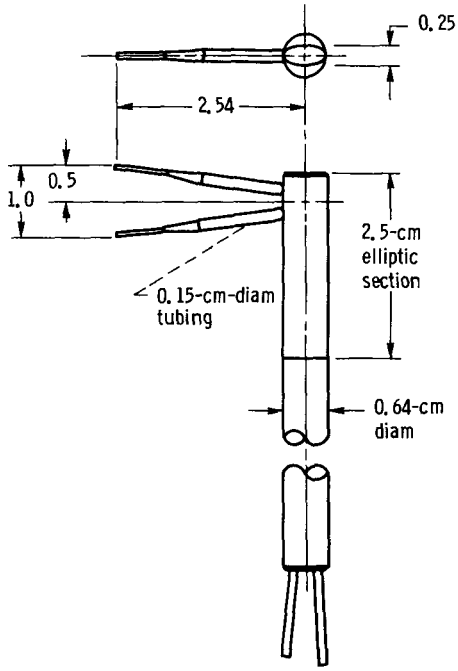

Figure 3. - Pressure and temperature survey probes. (Pressure probe tips are made of 0.07-mm-diam tubing with 60^{0} internal bevel for directional insensitivity. Temperature probe is similar except that the 0.07-mm-diam tubing is replaced with 0.05-mm-diam tubing having 0.025-mm-diam Chromel-Alumel spherical thermocouple junctions attached at the upstream ends.)

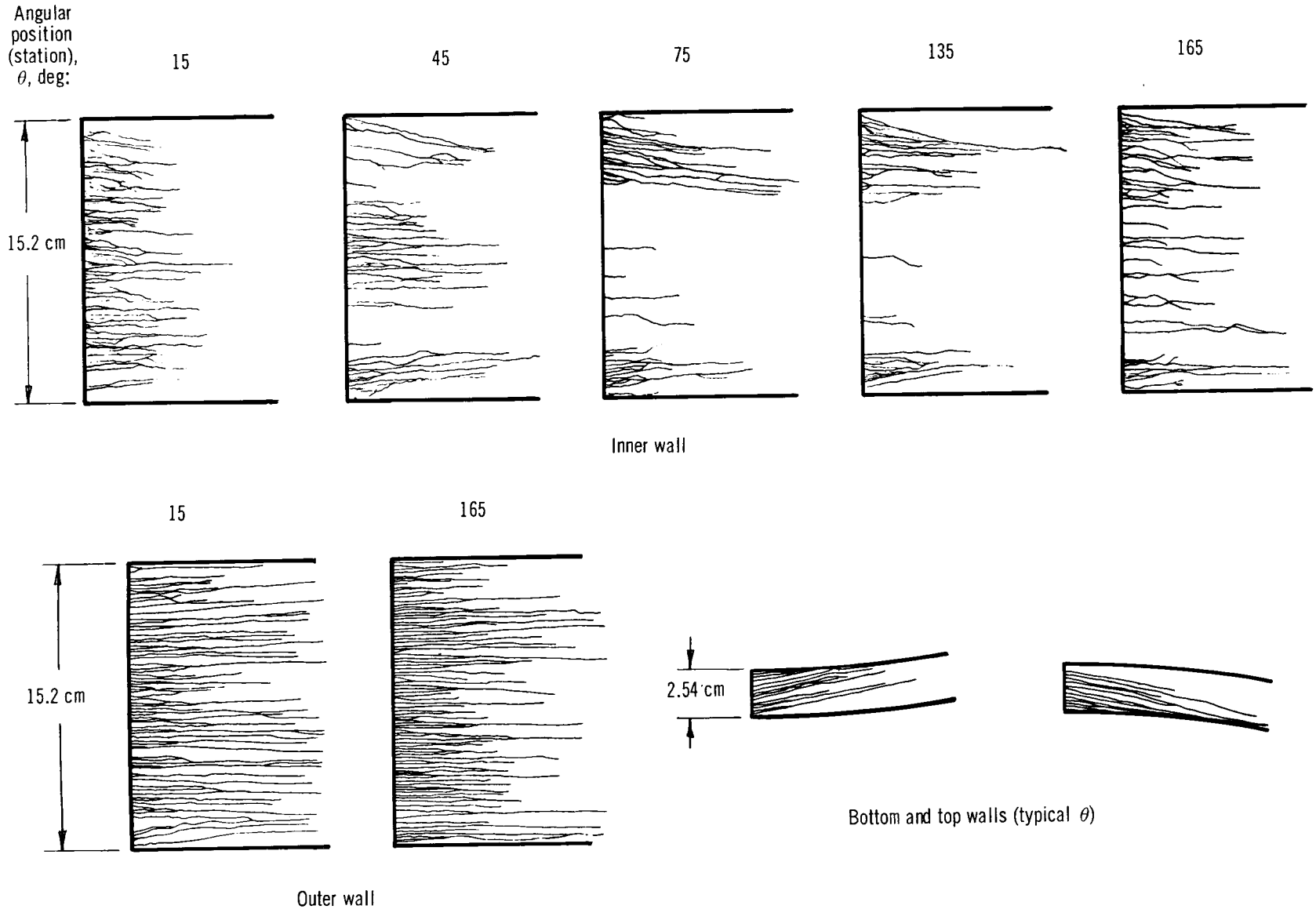

Figure 4. - Flow traces on walls of curved channel.

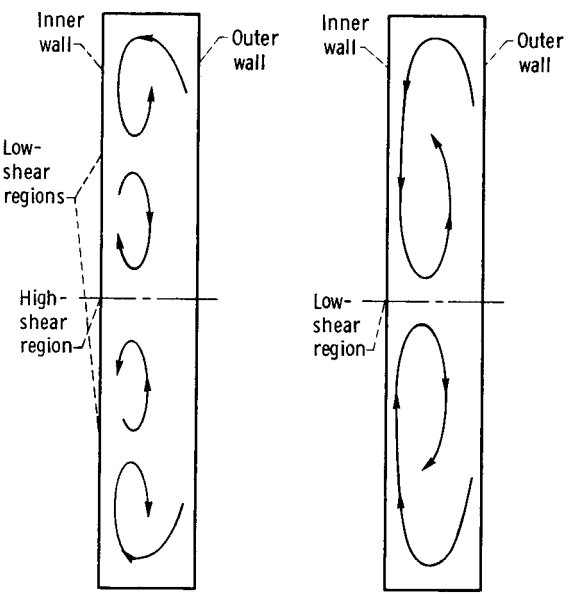

(a) Station θ, 15°. (b) Station θ, 75°.

Figure 5. - Inferred vortex patterns.

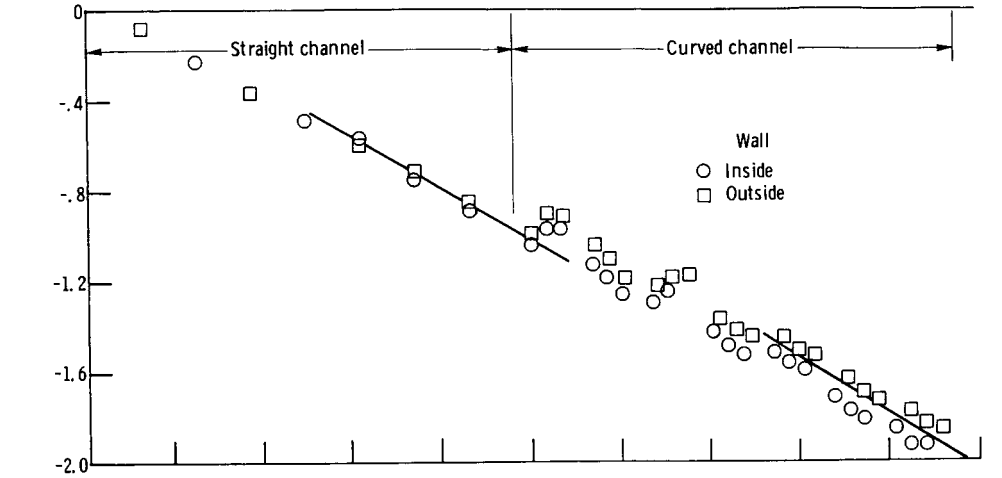

(a) Air inlet velocity, 30.5 meters per second.

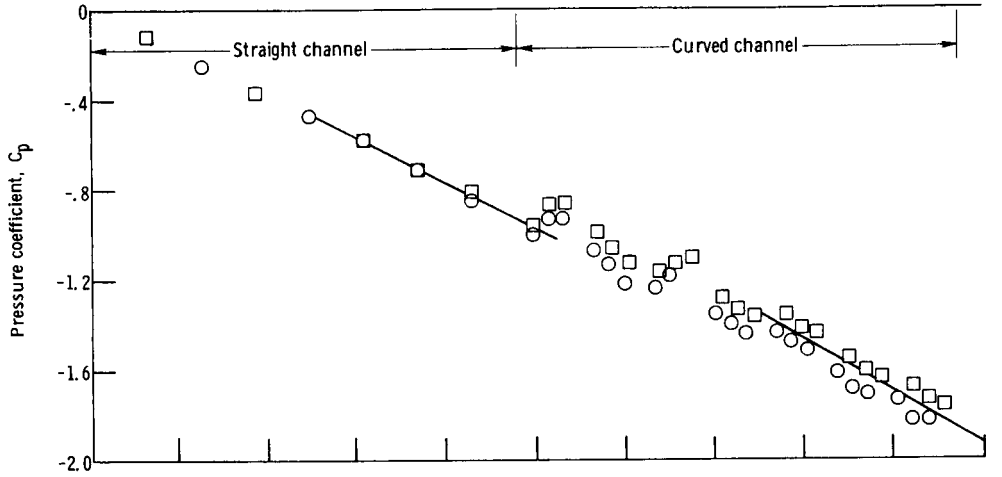

(b) Air inlet velocity, 61.0 meters per second.

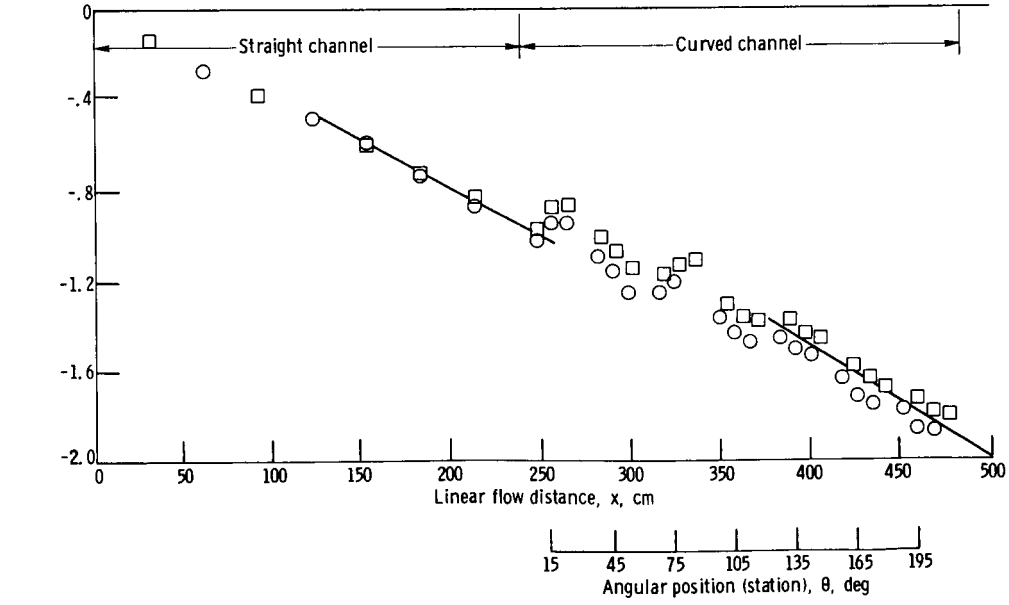

Pressure coefficient, C_p

(c) Air inlet velocity, 91.5 meters per second.

Figure 6. - Adiabatic pressure distribution.

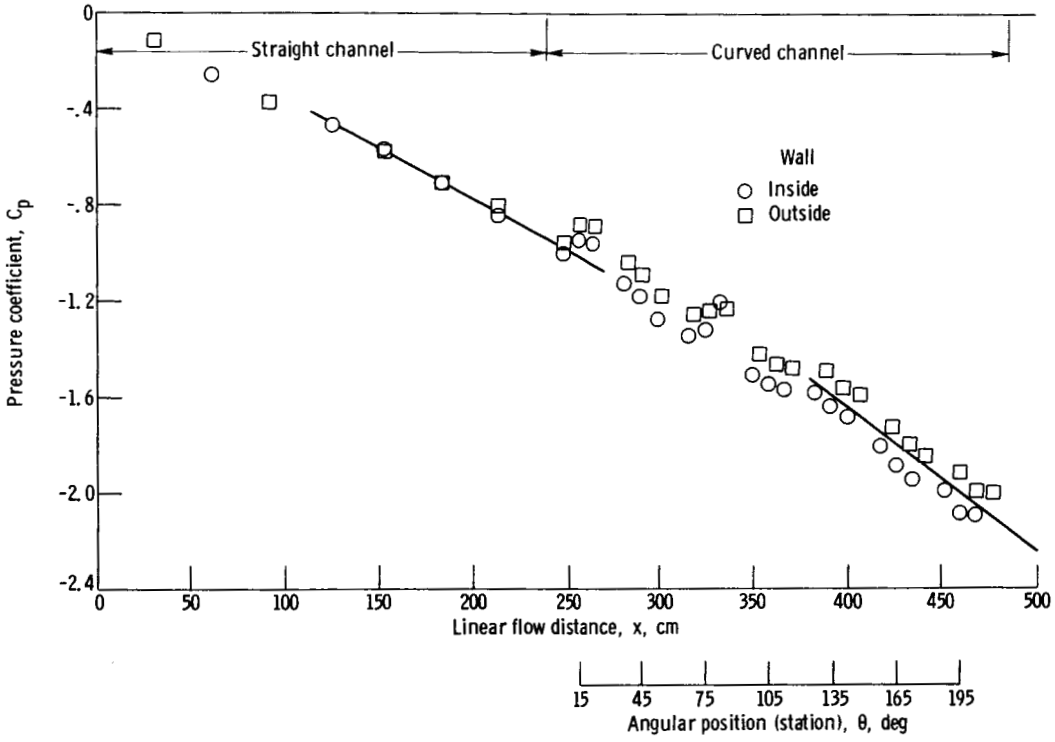

Figure 7. - Pressure distribution with both walls heated and air inlet velocity of 61.0 meters per second.

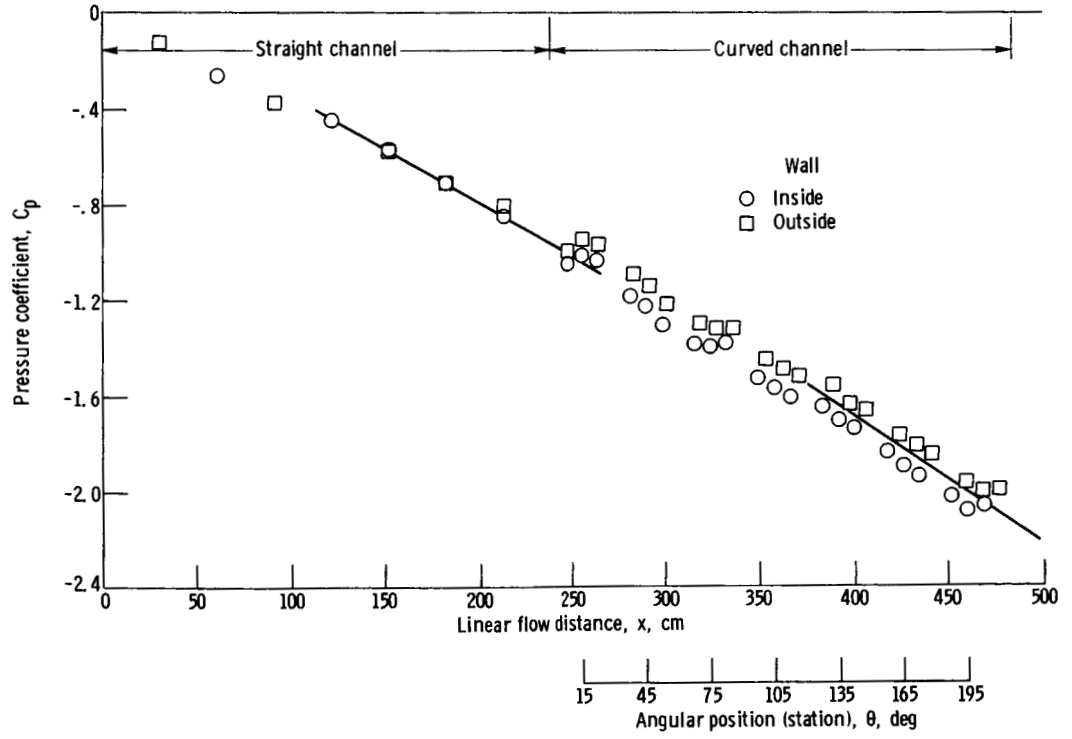

Figure 8. - Pressure distribution with inner wall heated and air inlet velocity of 61.0 meters per second.

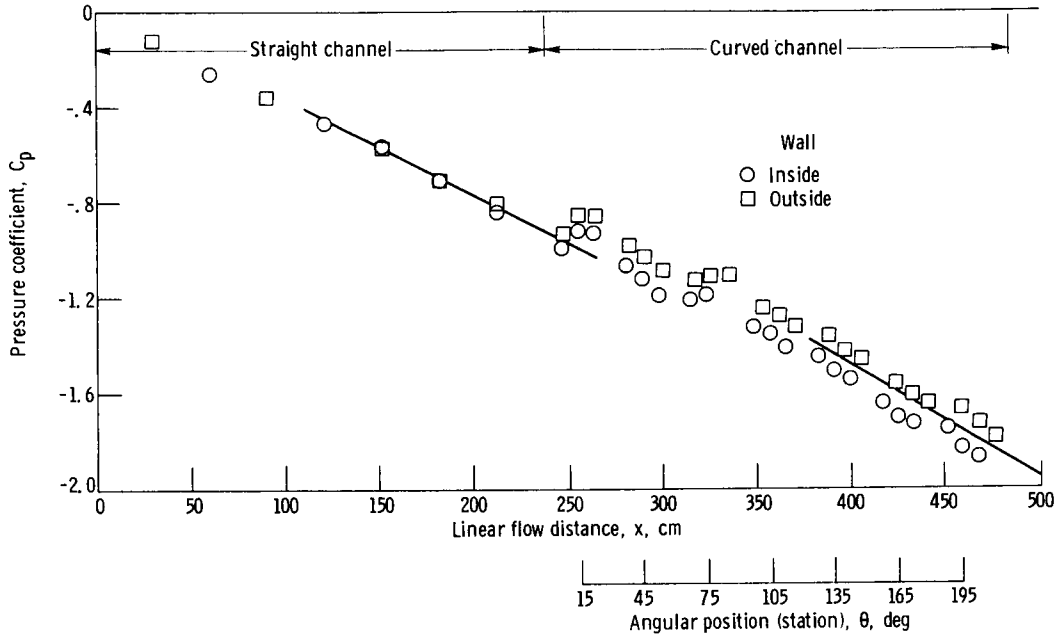

Figure 9. - Pressure distribution with outer wall heated and air inlet velocity of 61.0 meters per second.

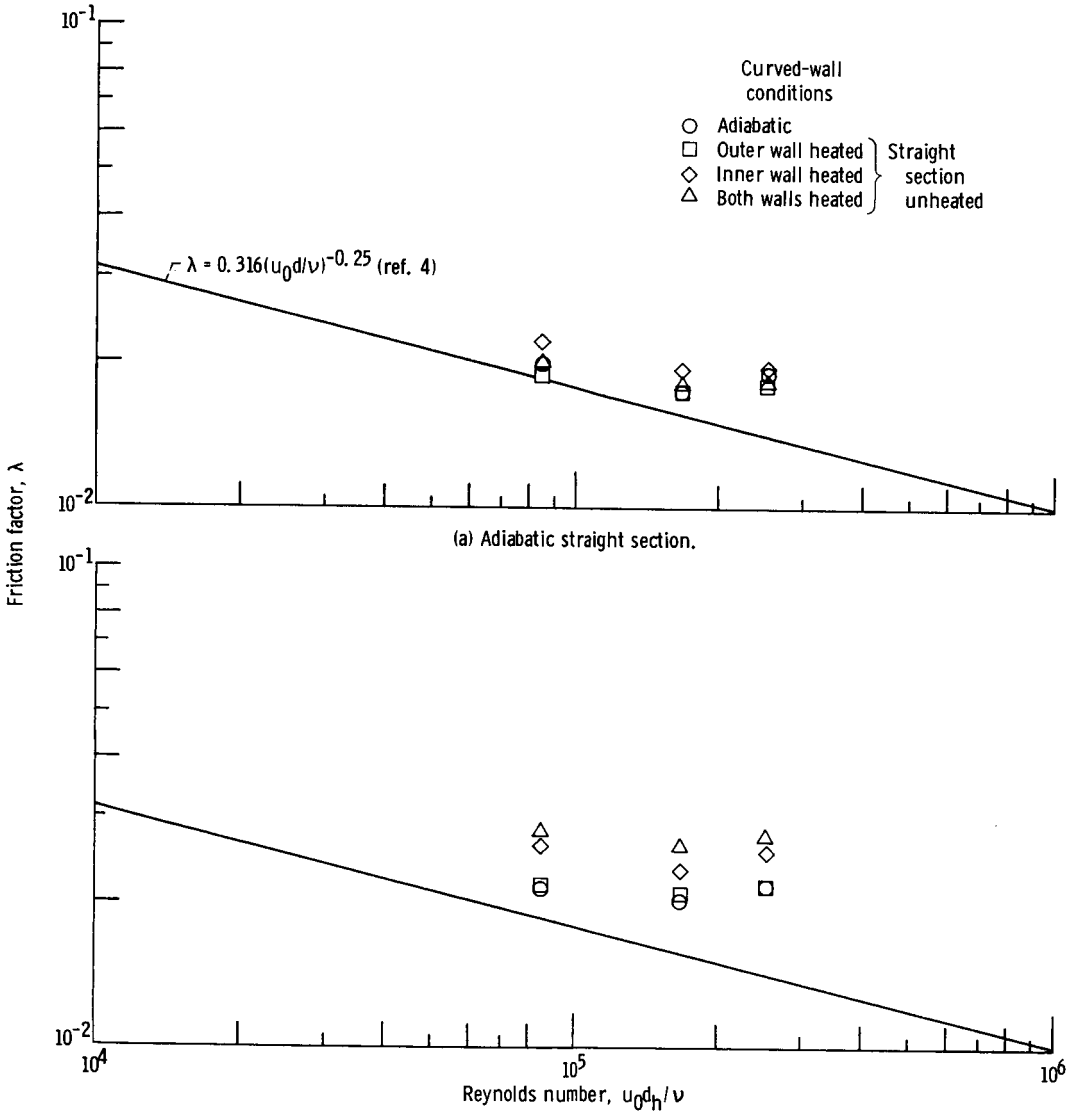

(a) Adiabatic straight section.

(b) Curved section.

Figure 10. - Friction factor.

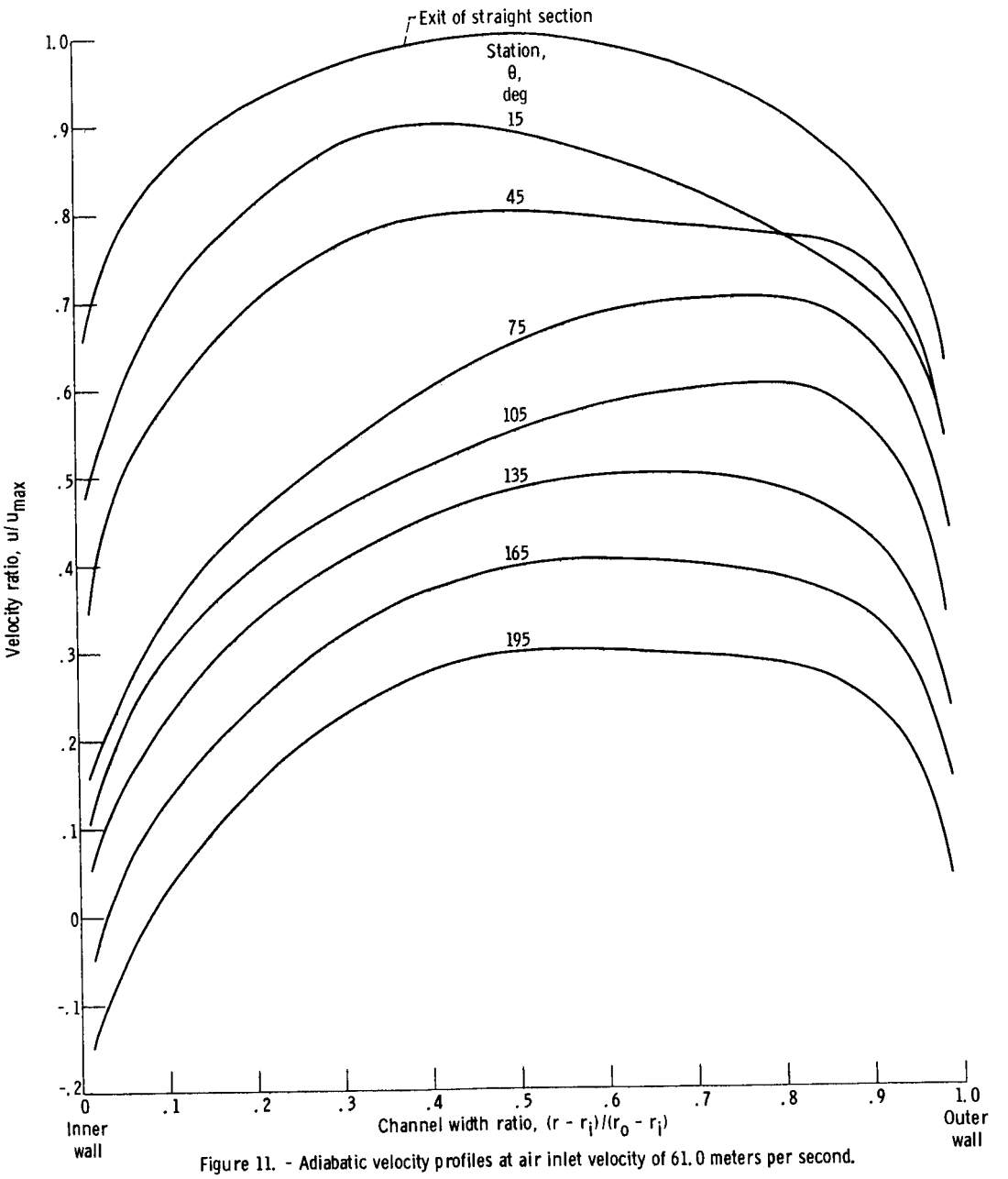

Figure 11. - Adiabatic velocity profiles at air inlet velocity of 61.0 meters per second.

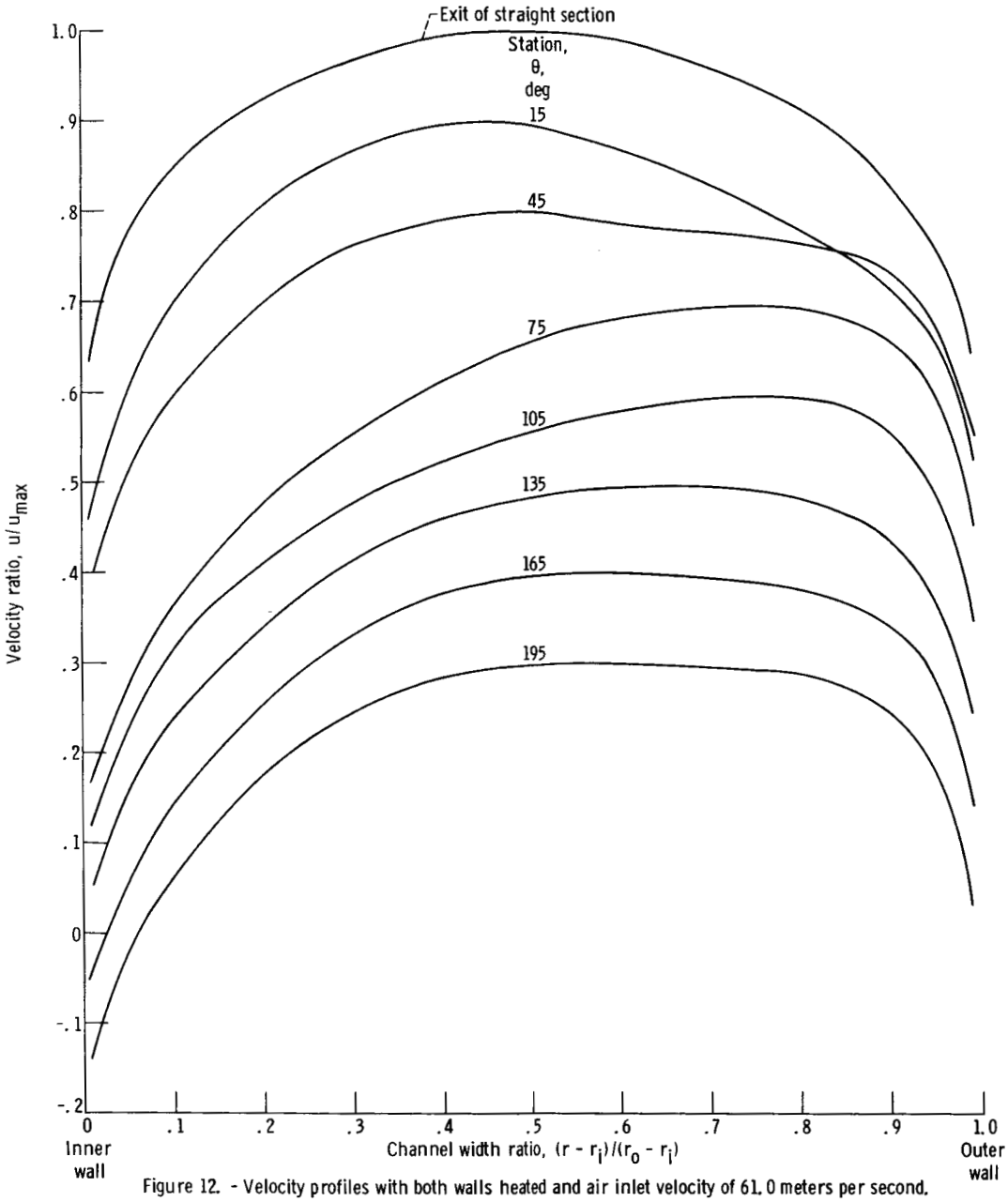

Figure 12. - Velocity profiles with both walls heated and air inlet velocity of 61.0 meters per second.

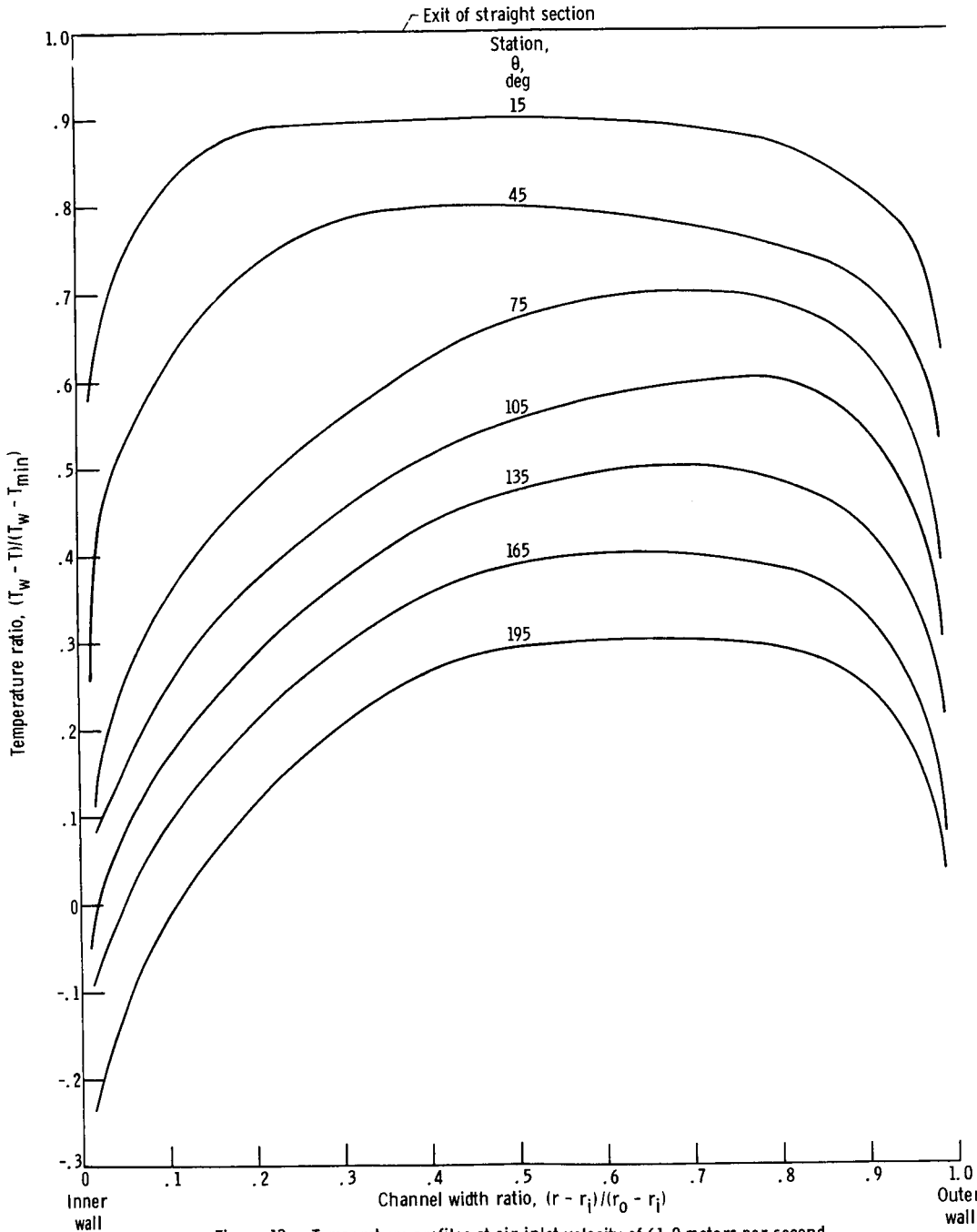

Figure 13. - Temperature profiles at air inlet velocity of 61.0 meters per second.

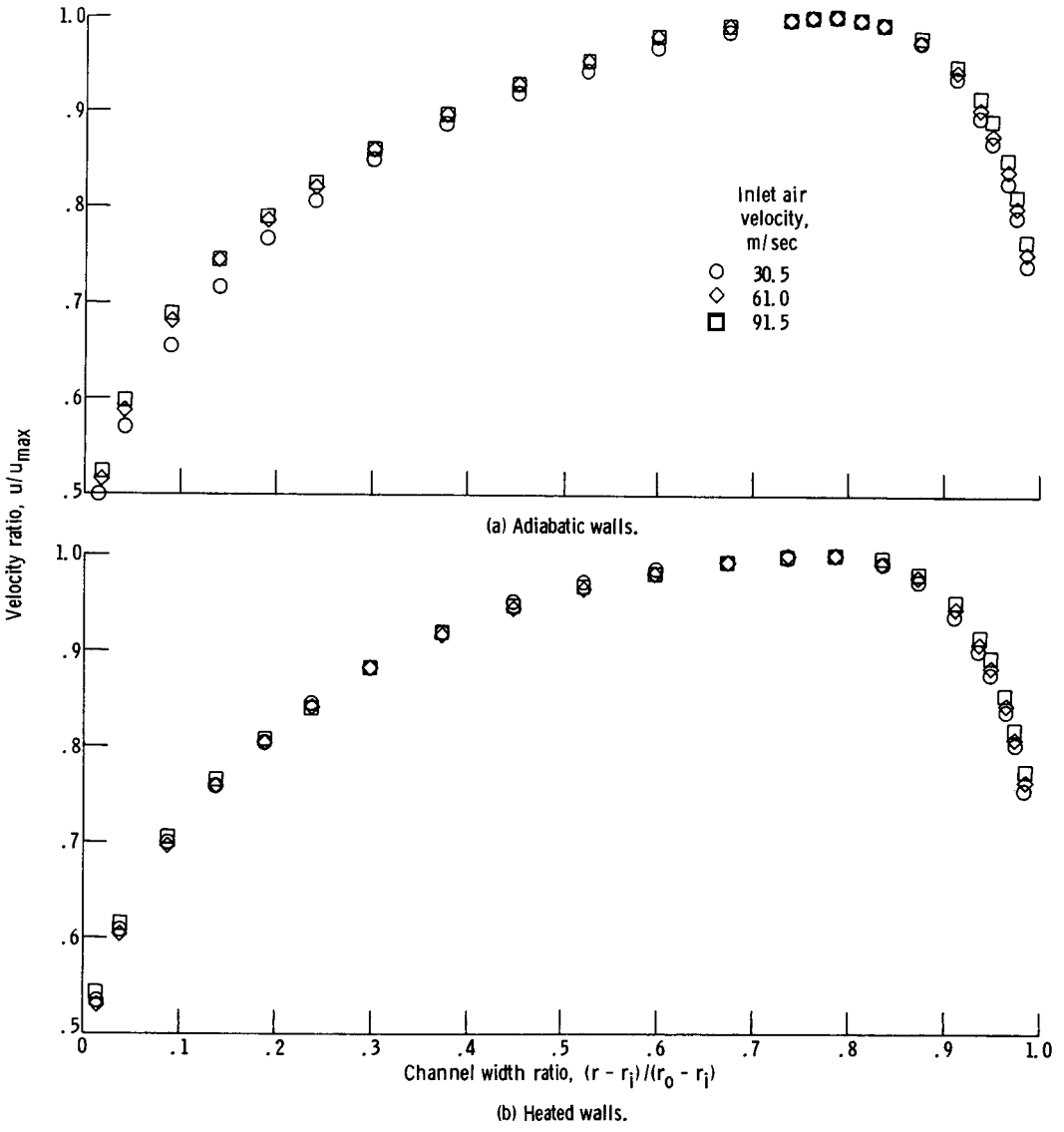

Figure 14. - Effect of air inlet velocity on velocity profile at 105° station.

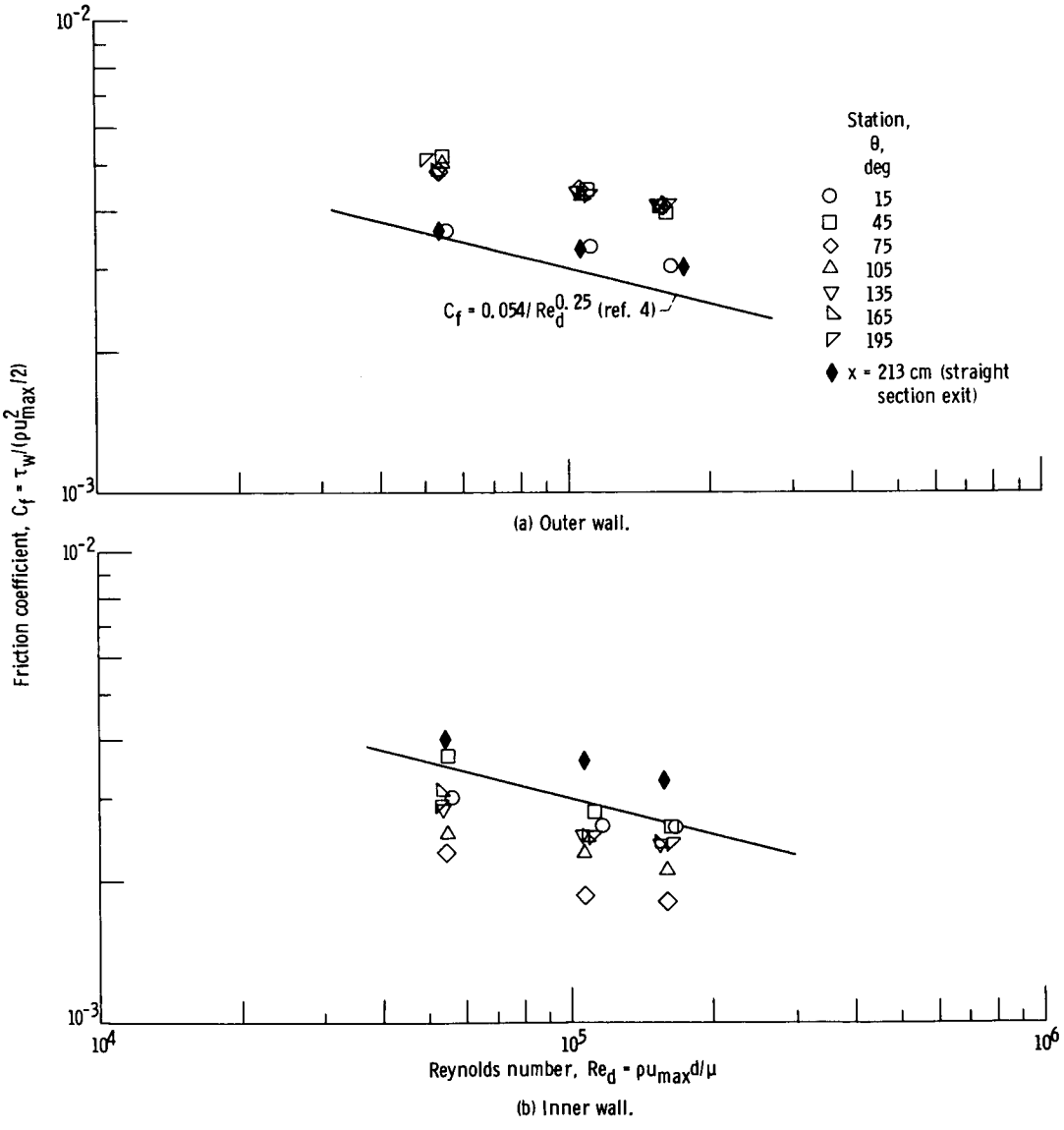

Figure 15. - Adiabatic Preston-tube friction measurements.

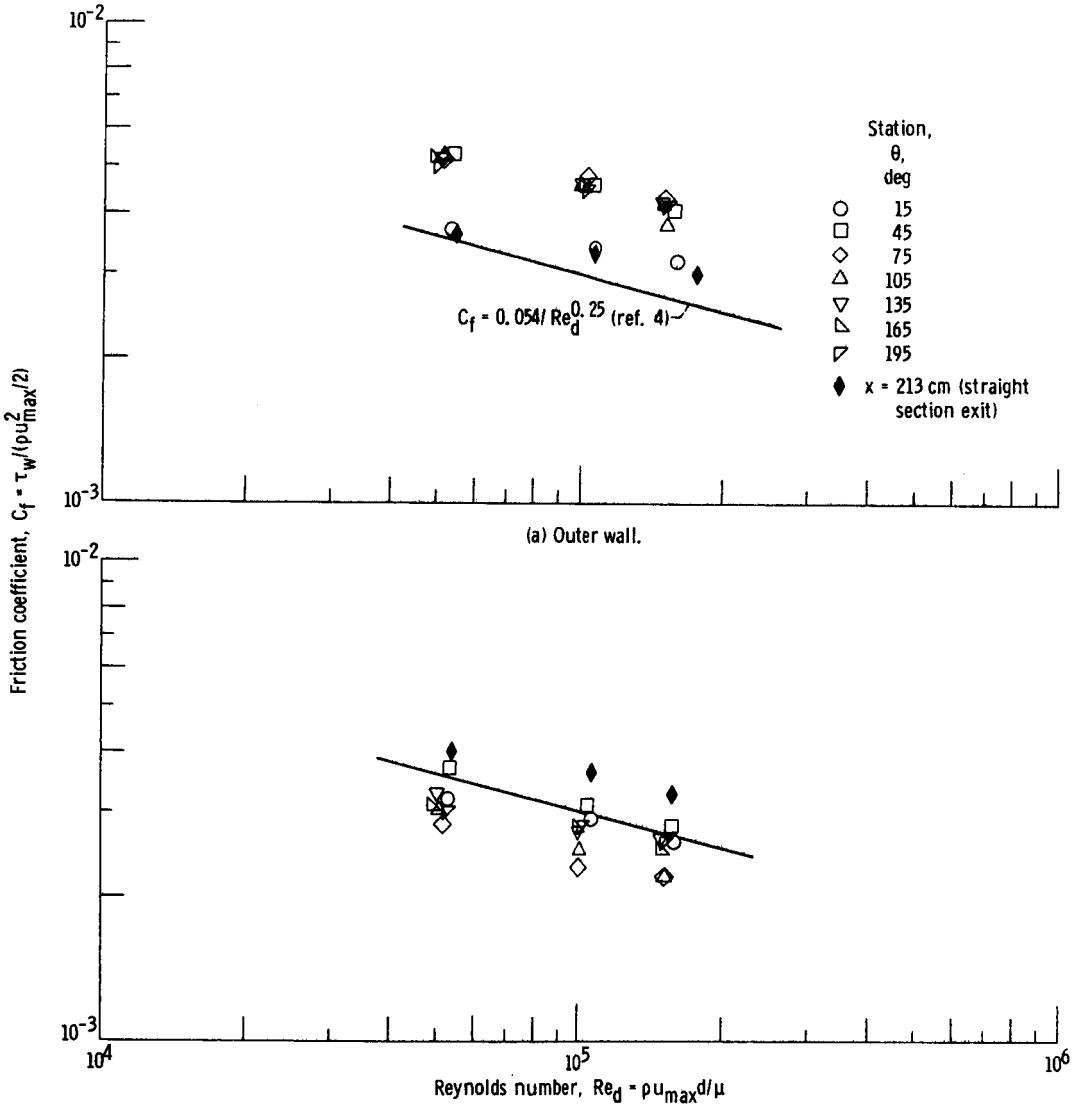

Figure 16. - Preston-tube friction measurements with heat transfer.

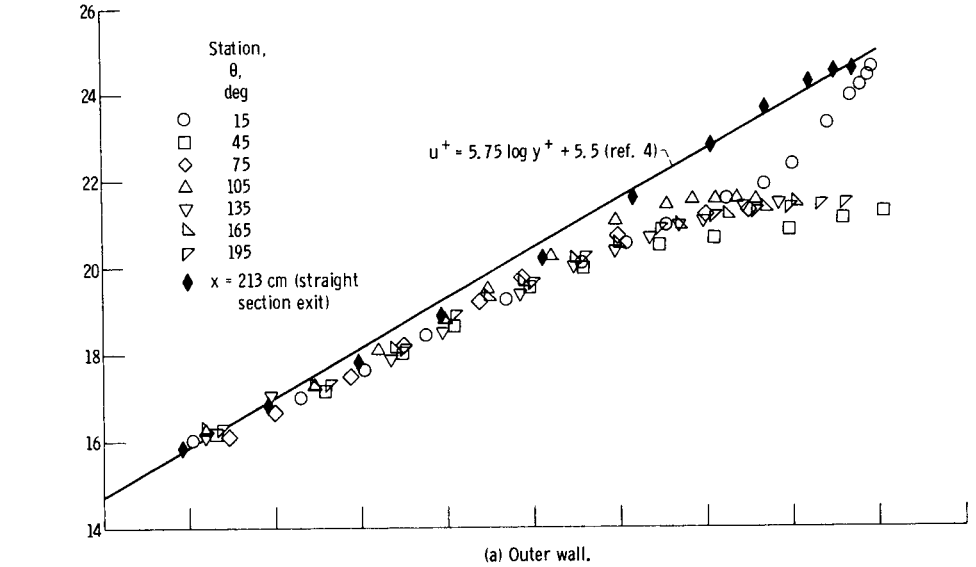

(a) Outer wall.

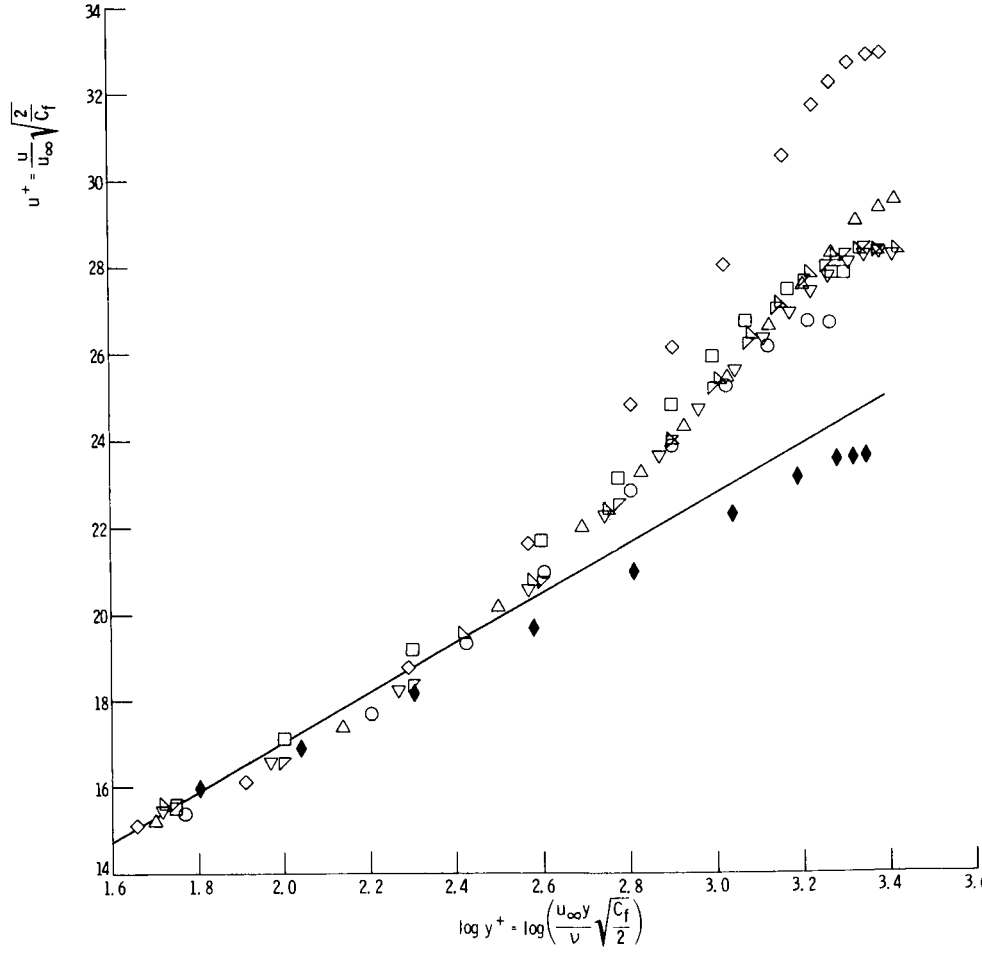

(b) Inner wall.

Figure 17. - Adiabatic velocity profiles at air inlet velocity of 61.0 meters per second.

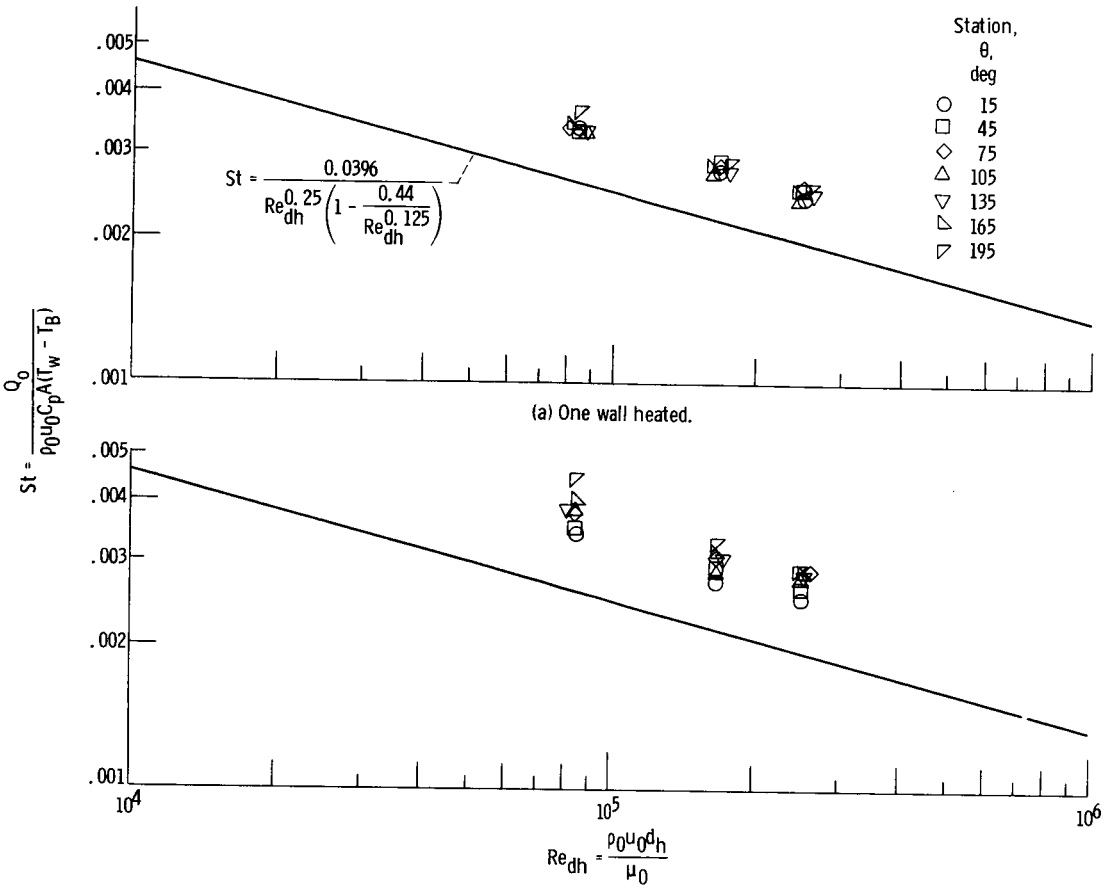

(a) One wall heated.

(b) Both walls heated.

Figure 18. - Outer-wall heat transfer.

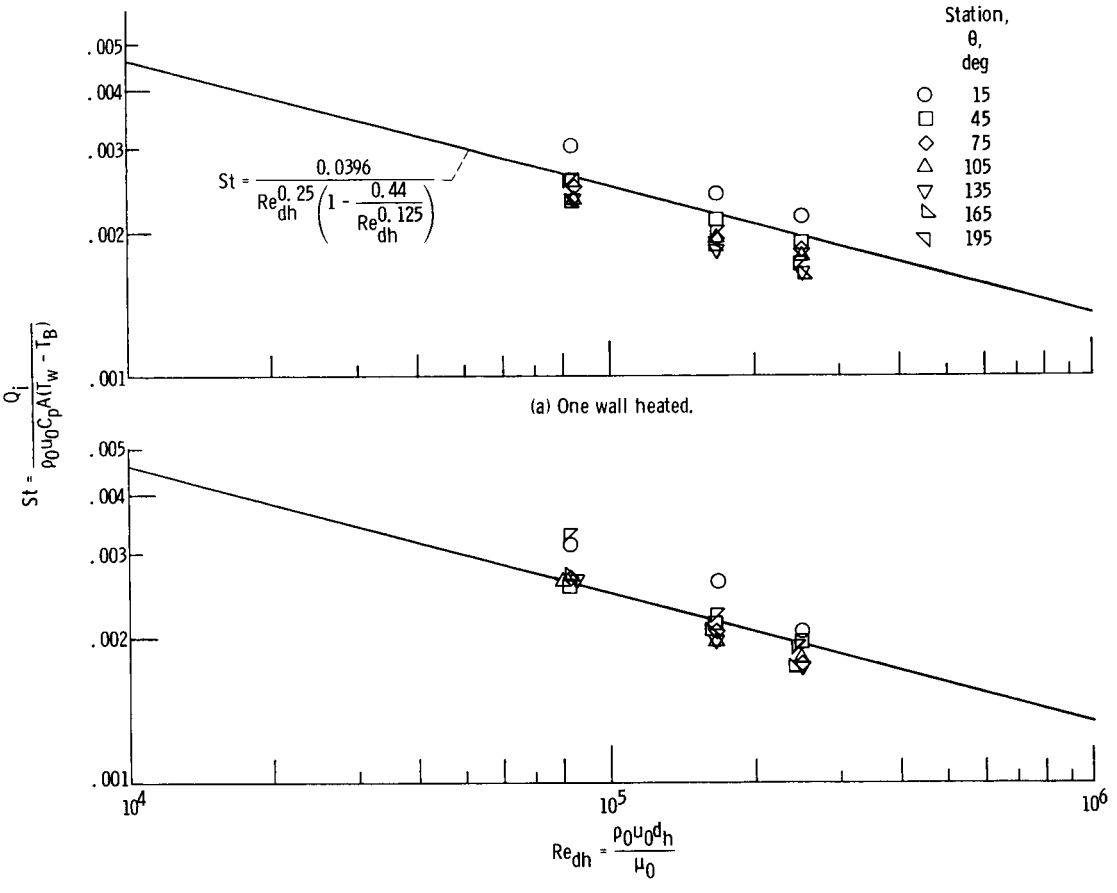

(a) One wall heated.

(b) Both walls heated.

Figure 19. - Inner-wall heat transfer.

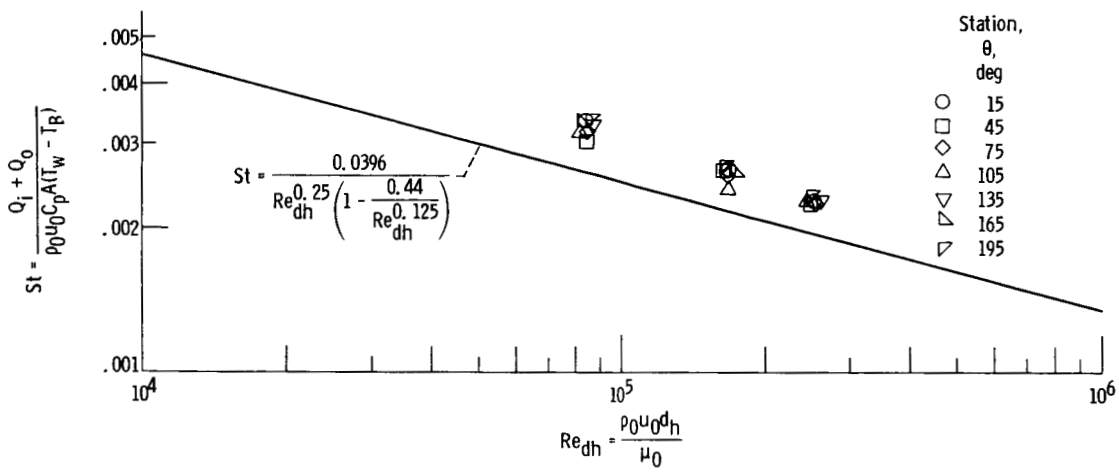

Figure 20. - Total heat transfer - both walls heated.

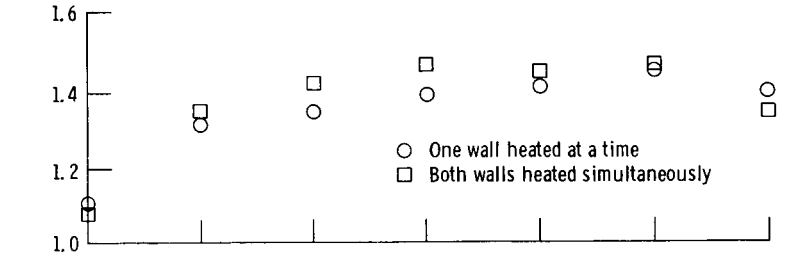

(a) Air inlet velocity, 30.5 meters per second; Reynolds number based on channel hydraulic diameter, Re_{dh}, 0.84×10^5.

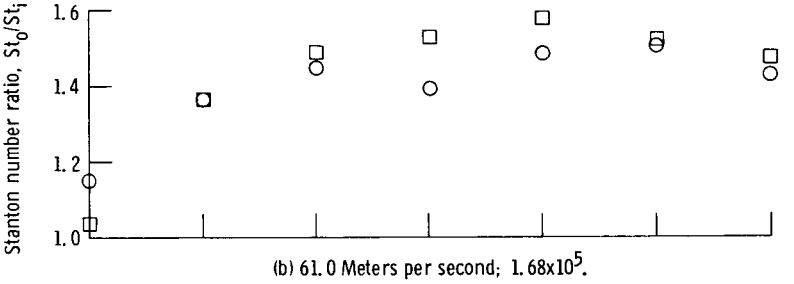

(b) 61.0 Meters per second; 1.68×10^5.

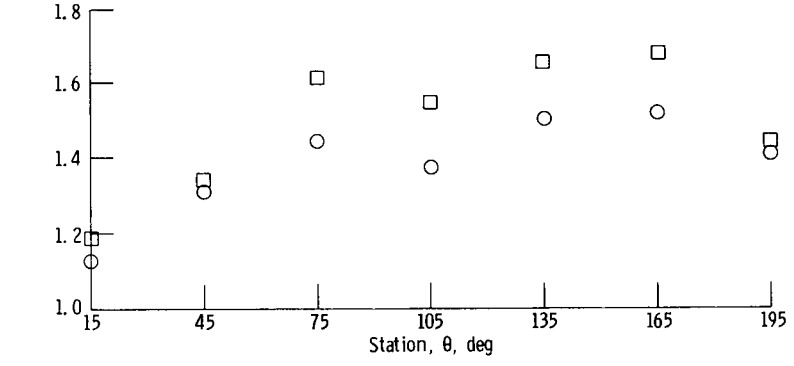

(c) 91.5 Meters per second; 2.53×10^5.

Figure 21. - Effect of angular position (station) on Stanton number ratio along curved channel.